Earthquakes and Structures, *Vol. 15, No. 6 (2018) 667-685*
DOI: https://doi.org/10.12989/eas.2018.15.6.667

Seismic behavior of K-type eccentrically braced frames with high strength steel based on PBSD method

Shen Li*[1], Chao-yu Wang[1], Xiao-lei Li[1], Zheng Jian[2] and Jian-bo Tian[2]

[1]*School of Civil Engineering and architecture, Xi'an University of Technology, Xi'an 710048, China*
[2]*State Key Laboratory Base of Eco-hydraulic Engineering in Arid Area, Xi'an University of Technology, Xi'an 710048, China*

(Received May 8, 2018, Revised October 17, 2018, Accepted November 19, 2018)

Abstract. In eccentrically braced steel frames (EBFs), the links are fuse members which enter inelastic phase before other structure members and dissipate the seismic energy. Based on the force-based seismic design method, damages and plastic deformations are limited to the links, and the main structure members are required tremendous sizes to ensure elastic with limited or no damage. Force-based seismic design method is very common and is found in most design codes, it is unable to determine the inelastic response of the structure and the damages of the members. Nowadays, methods of seismic design are emphasizing more on performance-based seismic design concept to have a more realistic assessment of the inelastic response of the structure. Links use ordinary steel Q345 (the nominal yielding strength f_y≥345 MPa) while other members use high strength steel (Q460 f_y≥460 MPa or Q690 f_y≥690 MPa) in eccentrically braced frames with high strength steel combination (HSS-EBFs). The application of high strength steels brings out many advantages, including higher safety ensured by higher strength in elastic state, better economy which results from the smaller member size and structural weight as well as the corresponding welding work, and most importantly, the application of high strength steel in seismic fortification zone, which is helpful to popularize the extensive use of high strength steel. In order to comparison seismic behavior between HSS-EBFs and ordinary EBFs, on the basis of experimental study, four structures with 5, 10, 15 and 20 stories were designed by PBSD method for HSS-EBFs and ordinary EBFs. Nonlinear static and dynamic analysis is applied to all designs. The loading capacity, lateral stiffness, ductility and story drifts and failure mode under rare earthquake of the designs are compared. Analyses results indicated that HSS-EBFs have similar loading capacity with ordinary EBFs while the lateral stiffness and ductility of HSS-EBFs is lower than that of EBFs. HSS-EBFs and ordinary EBFs designed by PBSD method have the similar failure mode and story drift distribution under rare earthquake, the steel weight of HSS-EBFs is 10%-15% lower than ordinary EBFs resulting in good economic efficiency.

Keywords: Eccentrically Braced Frames (EBFs); high strength steel; performance-based seismic design (PBSD); story drifts; failure mode

1. Introduction

The excellent hysteretic performance of eccentrically braced steel frames (EBFs) using shear links have made these systems an effective alternative for both moment-resisting frame as well as concentrically braced structures. The EBF system originated from Japan in 1970s (Fujimoto *et al*. 1972, Tanabashi *et al.* 1974) with the aim of achieving a structure with high elastic stiffness as well as high energy dissipation during severe earthquakes. The behavior of EBFs system with different brace patterns has been investigated (Azad and Topkaya 2017, Bosco and Rossi 2009, Lian *et al*. 2015, Lian and Su 2017, Wang *et al*. 2016, Tian *et al*. 2018), which depicted in Fig. 1 The successful behavior of EBFs under seismic loading depends on stable inelastic rotation of links and the ability of other frame members to facilitate these rotations. Therefore, during severe earthquakes, links can be considered as structural fuses which will dissipate the seismic input energy through stable and controlled plastic deformations (Engelhardt and Popov 2016, Hjelmstad and Popov 1983). The structure members expect links are designed oversize to ensure the links enter plastic deformations to dissipate seismic energy, so conventional EBFs is limited to application in building (Kuşyılmaz and Topkaya 2015). Moreover, it is possible that yielding in the shear links may not be uniformly distributed along the height of the structure and may be concentrated in a few floors causing excessive inelastic deformations at those levels by force-based seismic design (Richards 2014).

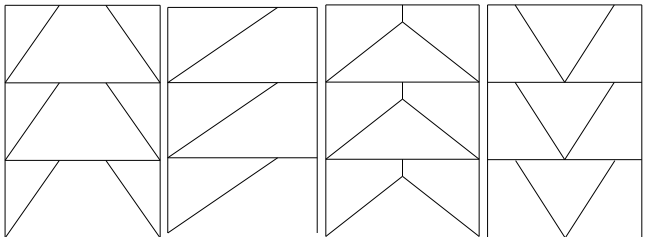

(a) *K*-type (b) *D*-type (c) *Y*-type (d) *V*-type

Fig. 1 The types of eccentrically braced steel frames

Eccentrically braced frames fabricated with high-strength steel (HSS-EBFs) are a new type of seismic

∗Corresponding author, Lecturer
E-mail: lishen2861@163.com

ISSN: 2092-7614 (Print), 2092-7622 (Online)

structural system. HSS-EBFs systems can incorporate Q345 steel (nominal yield strength: 345 MPa) for links, high strength steel (HSS) (nominal yield strength not less than 460 MPa) for beams and columns, and HSS or Q345 steel for braces. The application of high strength steels brings out many advantages, including higher safety ensured by higher strength in elastic state, better economy which results from the smaller member size and structural weight as well as the corresponding welding work, and most importantly, more environmental and ecological friendliness because of the less use of steels, welding and coating materials which means less consumptions of nonrenewable resources (Shi *et al*. 2014).

However, for HSS, the improved strength increases the ratio of the yield strength to tensile strength, which reduces the plastic deformation capacity. The requirements for steel use in seismic areas are clearly listed in the mandatory provisions of Chinese Code for Seismic Design of Buildings (GB50011-2010): the ratio of the measured yield strength to the measured tensile strength should not exceed 0.85, and the steel should have an obvious yield platform with an elongation ≥20%. Q460 or Q690 steel often fail to meet the above seismic requirements. These provisions limit the application of HSS in construction field of China. Nevertheless, the structures can meet the design concept of seismic codes by using reasonable structural type and structure details design (Dubina *et al*. 2015, Longo *et al*. 2014). Eccentrically braced frames (EBFs) with HSS are proposed to solve problem.

In this study a new design procedure based on energy and plastic design concepts is applied to HSS-EBFs, which called the performance-based seismic design (PBSD) method. The PBSD method begins by selecting a desired yield mechanism for the structure, which can predict and control inelastic deformation of structures by target drift and failure mode, and weak layers can be avoided. The design base shear and lateral forces are determined from input spectral energy for a given hazard level needed to push the structure in the yielded state up to a selected target drift. The desired yield mechanism for EBFs is all the inelastic deformations are isolated in the shear links in the form of shear yielding, since the plastic hinges developed at the column bases are almost inevitable in a severe earthquake, the story drifts for each story and the plastic rotations for each link are uniformly along the height of the structure.

In order to research the seismic behavior of HSS-EBFs compare with the ordinary EBFs, Four prototype structures with 5-, 10- , 15- and 20-story are assumed in high seismic risk zone. The HSS-EBFs and EBFs are designed by the PBSD method with the same target drift and yielding mechanism.

2. Experimental verification

A 1:2 scaled one-story one-bay *K*-type HSS-EBF specimen with a shear link was designed and applied for the experimental study of its hysteretic and monotonic performance. The story height and span of the specimen were 1.8 and 3.6 m, respectively. The length of shear link was 600 mm ($\rho=eV_p/M_p=1.45$; where, e, V_p, and M_p are the link length, plastic shear capacity, and plastic moment capacity, respectively), $\rho=1.45<1.6$, and the link is short (or shear yielding) in design.

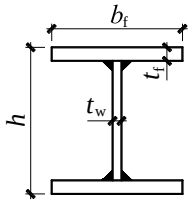

Fig. 2 Definition for the specimen sectional dimension

Table 1 Member sizes for the specimen

Member	Section (Chinese designation)
Beam	H225×125×6×10
Column	H150×150×6×10
Brace	H125×120×6×10
Link	H225×125×6×10

Table 2 Mechanical properties of steel

Steel	Q345B	Q345B	Q460C	Q460C
Thickness t (mm)	6	10	6	10
Yield stress f_y (Mpa)	427.40	383.33	496.90	468.77
Ultimate strength f_u (Mpa)	571.10	554.40	658.57	627.97
Yield strain ε_y($\times10^{-3}$)	2.12	1.92	2.39	2.32
Elastic modulus E ($\times10^5$MPa)	2.01	2.00	2.08	2.02
Elongation ratio (%)	26.53	31.01	29.73	35.88

Beams, columns, and braces were made of steel Q460 with nominal yield strength of 460 MPa, while the link was made of steel Q345 with nominal yield strength of 345 MPa. Welded joints were used to connect the link to the beam and the other members in the test specimen. The detailed member sections are listed in Table 1, the member sections are built-up section, and H-sections are used for the members, where"H" refers to the welded H-shaped section, the following numbers are section depth h, flange width b_f, web thickness t_w and flange thickness t_f, respectively (see Fig. 2) and the mechanical properties of the steel are presented in Table 2. The beam-column joint is a rigid connection, and the link and the frame beam are butt welded. Full-depth web stiffeners are provided on both sides of the link web and the link is provided with intermediate web stiffeners with the transverse stiffeners of spacing 150 mm, and the thickness of stiffener is 10 mm.

A vertical load of 800 kN is applied to the top of the column by a hydraulic jack to simulate the axial force transferred to the column by the superstructure. The actuator is connected to the reaction wall at one end, and the specimen is connected at the other end to exert the horizontal load. The lateral load is transferred to the frame column on the other side through the loading beam with the hinged connection and causes the synchronous lateral displacement of the frame on the left and right columns, thereby avoiding the influence of the transmission force of the link on the horizontal load transferring (Fig. 3). The

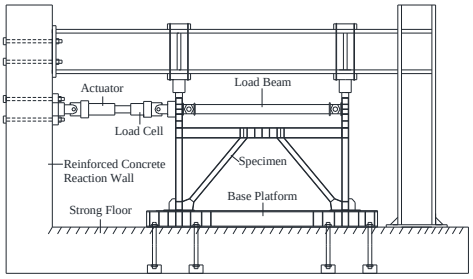

Fig. 3 Test setup

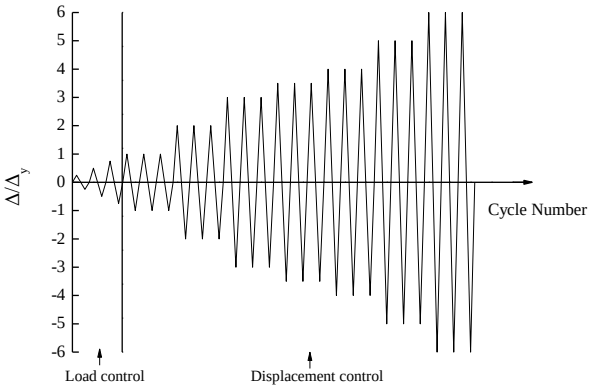

Fig. 4 Loading protocol

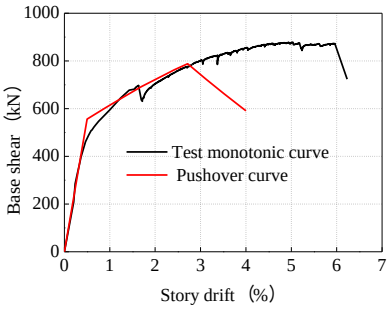

(a) Monotonic curve

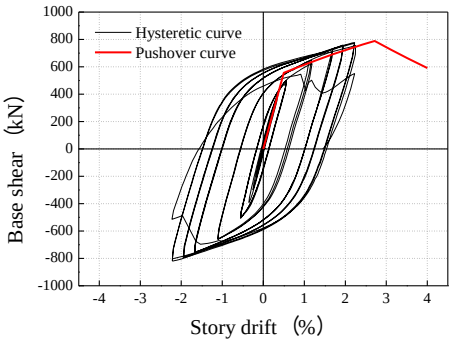

(b) Hysteretic curve

Fig. 5 Loading protocol

(a) Frame deformation

(b) Shear deformation of link

Fig. 6 Failure mode of monotonic test

loading test is monotonically loaded by the actuator at a loading speed of 0.05 mm/s until structural failure. The horizontal reciprocating loading is controlled by a combination of force and displacement in the pseudo-static test. The specimen is controlled by force before yielding, and then by displacements: $\pm\Delta_y$, $\pm2\Delta_y$, $\pm3\Delta_y$. $\pm4\Delta_y$, $\pm4.5\Delta_y$, and $\pm5.5\Delta_y$, where Δ_y is the yielding displacement. The specimens are subjected to one cycle per stage before yielding, followed by three displacement cycles until the specimen is destroyed. The loading protocol is depicted in Fig. 4

The SAP2000 finite element (FE) analysis software is used in this study to analyse the performance of *K*-EBFs fabricated with HSS. An FE model is developed, and the average values of flange and web plate properties are used as the material properties of each component. The two ends of the frame column are defined as *P*-*M* hinges, and both ends of the frame beam are defined as bending hinges (M3 hinge). The brace is axially loaded, the middle part is defined as the axial force hinge (*P* hinge), and the two ends and central part of the links are defined as plastic shear hinges (V2 hinge).

The pushover curve obtained from the pushover analyses of the FE models are compared with the test monotonic loading curves in Fig. 5. The hysteresis curves obtained by cyclic loading are shown in Fig. 5. The monotonic curve shows that *K*-type eccentrically braced structures exhibit excellent ductility and plastic deformation. The bearing capacity and stiffness of the specimens decreased with increasing plastic deformation of the link. The ultimate bearing capacity of specimen is approximately 825 kN, and the corresponding ultimate story drift is 3.33%, which exceeds the limit of the elastic-plastic story drift, that is 2%. The structure has excellent deformation capacity and ductility, the hysteresis loop is full and stable, and *K*-EBFs have excellent energy dissipation capacity. For the test specimen in the elastic state at the beginning of the loading, the hysteretic loop is long and narrow, and the specimen only marginally dissipates energy, and the hysteretic circuit gradually opens and tends to be fully when the link in the elastic-plastic state.

The failure modes of the specimens from the monotonic and hysteretic test are shown in Figs. 6 and 7. The failure

(a) Frame deformation

(b) Shear deformation of link

Fig. 7 Failure mode of hysteresis test

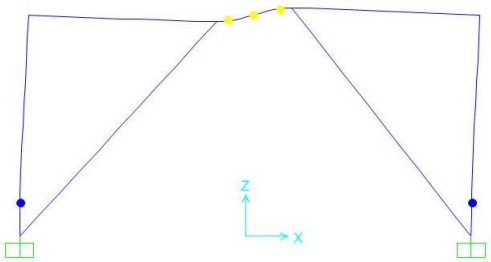

Fig. 8 Failure mode of FE model

mode of FE model from the pushover analysis is shown in Fig. 8. The failure model for FE model is similar with the monotonic test. When the frame drift is more significant than $H/50$ (H is the height of the structure), the deformation of the link reaches the plastic limit state (as per GB50011-2010), the shear hinge unloads, and the pushover curves exhibit a downward trend. The components in SAP2000 are truss elements, the average value material properties of the flanges and web plates were taken as the material model, and the plastic deformation of the structure was concentrated in the plastic hinges by defining the plastic behavior of the plastic hinge reaction structure. When the plastic hinge of the structure reaches the limit state in the FE model, unloading of the hinge occurs, causing the bearing capacity to rapidly decrease. The line element is used for beam and column in FE model, and that the plastic zone is just a point, it is a difference with the actual structure, which is the primary cause of errors.

3 Finite element analysis

3.1 Performance-based seismic design method

With the development of seismic design theory, seismic designs of structures have gradually changed from strength-based to performance-based design methods. The PBSD method of EBFs has been investigated in previous study (Li *et al*. 2017). The PBSD method concept has a more realistic assessment of the inelastic response of the structures. This method is based on the energy equilibrium between inelastic displacement of a structure and presumed yielding mechanism, where the links are the dissipative members,

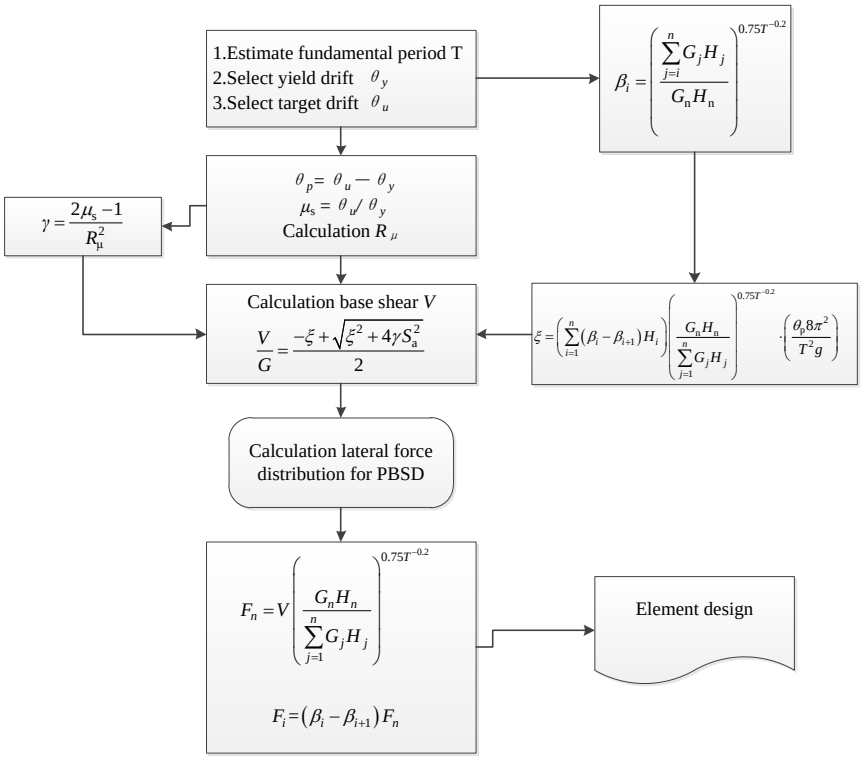

Fig. 9 Performance-based plastic design flowchart: design base shear and lateral force distribution

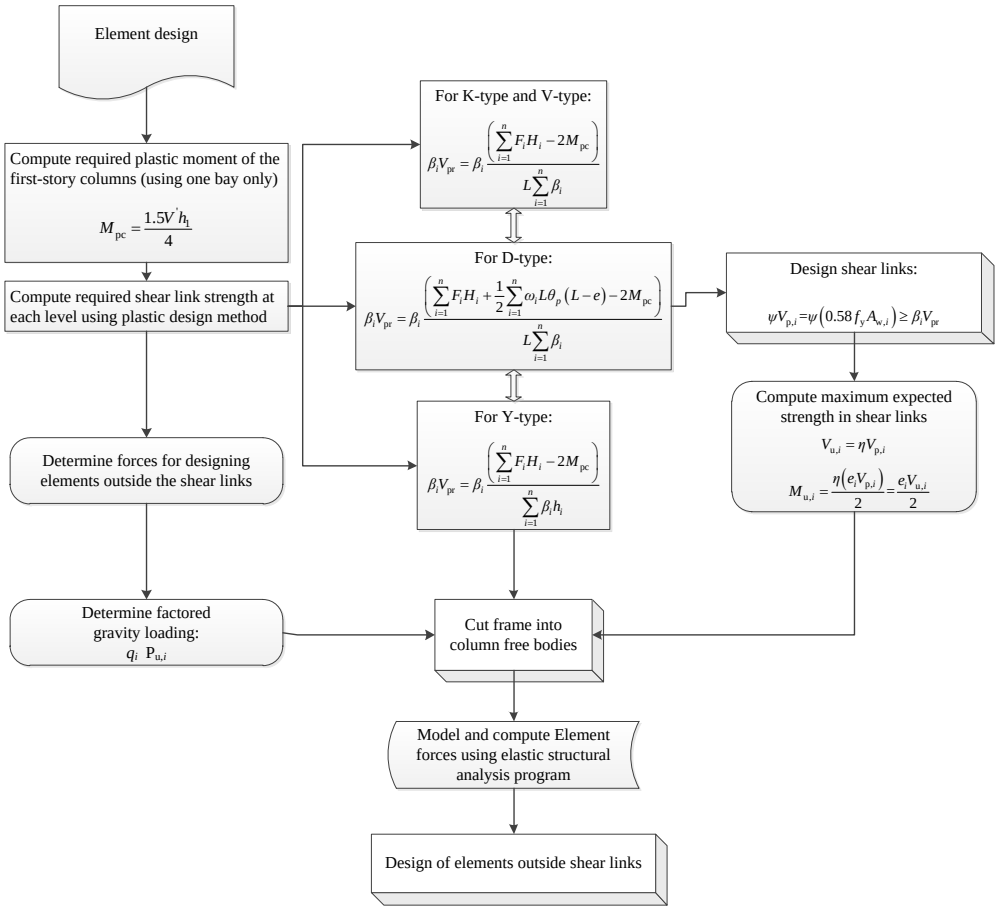

Fig. 10 Performance-based plastic design flowchart for EBF: element design

and the non-energy dissipation members are in an elastic state when the structure fails in an earthquake, the story drift is uniform, and no weak story appears. The PBSD takes the yielding and ultimate displacement of the structure as the performance target, and the ideal failure mode of the structure as the performance limit state during an earthquake. The design flow charts are presented in Fig.9 and 10. Both the HSS and ordinary steel K-EBFs designed by the PBSD exhibit similar performance objectives and failure modes, and their seismic performance will now be compared.

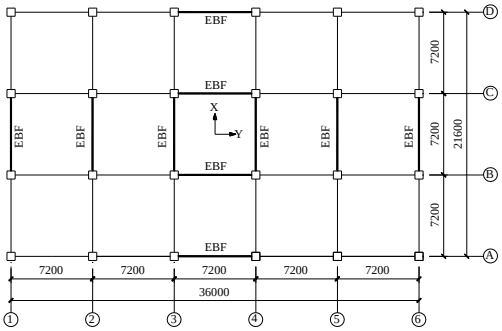

Fig. 11 The plan view of 5-story building (mm)

3.2 Prototype overview

The prototypes design includes four groups: 5-stories, 10-stories, 15-stories, and 20-stories. The links and braces were used for Q345 (f_y=345 MPa) steel, and the beams and columns for Q460 (f_y=460 MPa) steel in the *K*-EBF with HSS models. The K-EBFs with ordinary steel were all manufactured from Q345 steel. The material yield strengths used were the nominal values, and the elastic modulus used was 2.06×10^5 MPa. In the following expressions, the *K*-EBFs with ordinary steel are represented by OK, and those with HSS are represented by HK. For example, OK-S5 represents 5-story *K*-EBF with ordinary steel. The design models are characterized by a peak ground acceleration of 0.3 g with a 10% probability of exceedance over a 50-year period, and moderately firm ground conditions. The factor that reduces the elastic response spectrum to obtain the design spectrum is 2.8125 in GB50011-2010(Code for seismic design of buildings in Chinese). The alpha damping, α, and beta damping, β, were specified according to the damping, ζ, and the fundamental period of the structures. In addition, damping of 4% is considered appropriate for a steel building with a structural height not exceeding 50 m, and 3% for structural heights between 50-200 m according to the requirements of GB50011-2010. In all design examples, the concrete floor slab is 120 mm thick, and cast-in-place. The constraints between the columns of different stories were continuous, and rigid connections were used between columns and beams in all design examples. Box sections were used for the frame columns, and welded H-sections for the other members. The

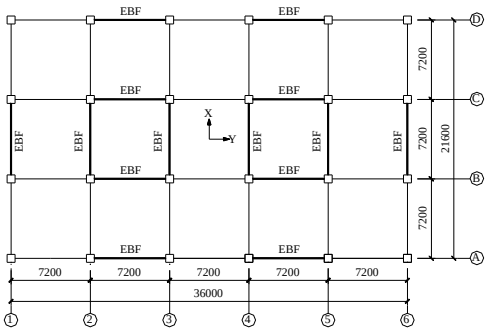

Fig. 12 The plan view of 10-story building (mm)

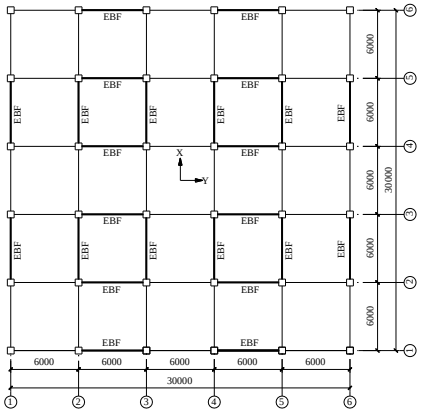

Fig. 13 The plan view of 15-story building (mm)

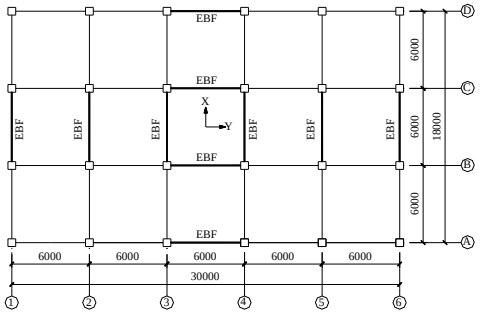

Fig. 14 The plan view of 20-story building (mm)

dead load on the floor was 5.0 kN/m^2, that including the floor weight, the floor live load was 2.0 kN/m^2, the roof dead load was 6.0 kN/m^2, the roof live load was 2.0 kN/m^2, the snow load was 0.35 kN/m^2, and the basic wind pressure was 0.35 kN/m^2. The plan view of prototypes is shown in Figs. 11-14. For 5-story building, there are five bays in the *X*-direction for one-bay EBF and three bays in the *Y*-direction for one-bay EBF, the spans in both the *X*- and *Y*-directions are 7.2 m, The plan view of 10-story building is similar with 5-story, the difference is *Y*-direction has two-bay EBF. The length of the link is 900mm and the story height is 3.3 m for 5-story and 10-story buildings. For 15-story building, there are five bays in *X*- direction and *Y*-direction for two EBFs, and the spans are 6.0 m in both the *X*- and *Y*-directions, all links' are 800 mm and the story height is 3.3 m, therefore the cross-section of members for *X* and *Y*-directions are the same. The plan layout of 20-story building is same with 5-story buildings, and the spans are 6.0 m, the length of link is 600 mm for *X*-direction and 700 mm for *Y*-direction. The structural height of 20-story building is 70.8 m, and 4.5 m for 1-4 each story and 3.3 m for others.

Table 3 Member sections of OK-S5

Story	Beams in *X*-direction	Beams in *Y*-direction	Links in *X*-direction	Links in *Y*-direction	Column	Brace
5	H370×150×8×12	H360×130×6×10	H300×140×6×12	H370×160×6×12	□350×350×16	H200×200×10×18
4	H400×200×10×16	H440×150×8×12	H390×160×8×14	H400×180×10×16	□420×420×16	H220×220×10×18
3	H460×230×10×16	H400×180×10×16	H420×180×10×16	H520×180×10×16	□450×450×16	H250×250×10×18
2	H510×230×10×16	H450×180×10×16	H480×180×10×16	H500×200×12×18	□500×500×16	H250×250×10×18
1	H540×230×10×16	H470×180×10×16	H510×180×10×16	H540×200×12×18	□500×500×16	H250×250×10×18

Table 4 Member sections of HK-S5

Story	Beams in *X*-direction	Beams in *Y*-direction	Links in *X*-direction	Links in *Y*-direction	Column	Brace
5	H310×140×6×12	H300×130×6×12	H310×140×6×12	H280×140×8×12	□300×300×16	H200×200×10×18
4	H370×160×10×16	H340×160×8×12	H400×160×8×14	H400×180×10×16	□350×350×16	H220×220×10×18
3	H430×180×10×16	H420×160×8×12	H430×180×10×16	H520×180×10×16	□400×400×16	H250×250×10×18
2	H480×180×10×16	H390×180×10×14	H490×180×10×16	H500×200×12×18	□460×460×16	H250×250×10×18
1	H510×180×10×16	H410×180×10×14	H520×180×10×16	H540×200×12×18	□460×460×16	H250×250×10×18

Table 5 Member sections of OK-S10

Story	Beams in *X*-direction	Beams in *Y*-direction	Links in *X*-direction	Links in *Y*-direction	Column	Brace
10	H360×170×6×12	H320×150×6×12	H330×160×6×12	H280×140×6×12	□400×400×16	H220×220×10×16
9	H410×200×10×16	H390×150×10×16	H360×180×10×16	H340×160×8×14	□450×450×16	H220×220×10×16
8	H520×200×10×16	H410×200×10×16	H470×180×10×16	H450×160×8×14	□500×500×18	H240×240×12×18
7	H550×200×12×18	H480×200×10×16	H480×200×12×18	H440×180×10×16	□500×500×18	H240×240×12×18
6	H550×240×12×18	H490×230×10×16	H540×200×12×18	H500×180×10×16	□600×600×18	H260×260×12×18
5	H550×240×14×20	H530×230×10×16	H520×240×14×20	H550×180×10×16	□600×600×18	H280×280×12×18
4	H580×240×14×20	H550×240×10×16	H560×240×14×20	H500×200×12×18	□670×670×22	H280×280×12×18
3	H600×240×14×20	H570×240×10×16	H590×240×14×20	H530×200×12×18	□670×670×22	H280×280×12×18
2	H610×240×14×20	H580×240×10×16	H600×240×14×20	H540×200×12×18	□750×750×24	H280×280×12×18
1	H620×240×14×20	H590×240×10×16	H610×240×14×20	H550×200×12×18	□750×750×24	H280×280×12×18

3.3 Member section

The yield and ultimate drift are regarded as the performance design parameter of the PBSD method, and the ideal failure mode is taken as the performance limit state. Each story of link deforms to dissipate energy, the story drift distribution along the structure height is uniform, and plastic hinges appear at the end of the column base to reach the ultimate state. The section sizes of the four *K*-EBF groups designed by the PBSD method are presented in Tables 3-10, where OK-S5 and HK-S5 are 5-story *K*-EBFs

Table 6 Member sections of HK-S10

Story	Beams in *X*-direction	Beams in *Y*-direction	Links in *X*-direction	Links in *Y*-direction	Column	Brace
10	H320×150×6×12	H300×120×6×12	H300×160×8×14	H280×140×6×12	□300×300×16	H220×220×10×16
9	H400×150×10×16	H360×150×8×14	H370×160×10×16	H350×160×8×14	□350×350×16	H220×220×10×16
8	H440×200×10×16	H400×150×10×16	H490×180×10×16	H380×180×10×16	□400×400×16	H240×240×12×18
7	H500×200×10×16	H470×150×10×16	H500×200×12×18	H460×180×10×16	□400×400×16	H240×240×12×18
6	H530×220×10×16	H440×200×10×16	H570×200×12×18	H520×180×10×16	□450×450×16	H260×260×12×18
5	H490×240×12×18	H480×200×10×16	H540×240×14×20	H490×200×12×18	□450×450×16	H280×280×12×18
4	H520×240×12×18	H500×200×10×16	H580×240×14×20	H520×200×12×18	□550×550×20	H280×280×12×18
3	H540×240×12×18	H520×200×10×16	H610×240×14×20	H550×200×12×18	□550×550×20	H280×280×12×18
2	H550×240×12×18	H500×220×10×16	H630×240×14×20	H560×200×12×18	□610×610×22	H280×280×12×18
1	H560×240×12×18	H510×220×10×16	H640×240×14×20	H570×200×12×18	□610×610×22	H280×280×12×18

Table 7 Member sections of OK-S15

Story	Beams in *X*-direction	Beams in *Y*-direction	Links in *X*-direction	Links in *Y*-direction	Column	Brace
15	H340×100×6×10	H340×100×6×10	H300×150×6×12	H300×150×6×12	□250×250×12	H180×180×10×16
14	H340×150×8×14	H340×150×8×14	H300×150×8×14	H300×150×8×14	□300×300×12	H180×180×10×16
13	H400×170×8×14	H400×170×8×14	H380×160×10×16	H380×160×10×16	□300×300×12	H200×200×10×16
12	H420×200×8×14	H420×200×8×14	H380×180×10×16	H380×180×10×16	□400×400×16	H200×200×10×16
11	H420×200×10×16	H420×200×10×16	H430×180×10×16	H430×180×10×16	□400×400×16	H220×220×10×16
10	H460×200×10×16	H460×200×10×16	H480×180×10×16	H480×180×10×16	□450×450×18	H220×220×10×16
9	H500×200×10×16	H500×200×10×16	H520×180×10×16	H520×180×10×16	□450×450×18	H240×240×10×16
8	H520×200×10×16	H520×200×10×16	H470×200×12×18	H470×200×12×18	□550×550×18	H250×250×10×16
7	H500×230×10×16	H500×230×10×16	H500×200×12×18	H500×200×12×18	□550×550×18	H250×250×10×16
6	H510×240×10×16	H510×240×10×16	H520×200×12×18	H520×200×12×18	□650×650×20	H250×250×10×16
5	H520×240×10×16	H520×240×10×16	H540×200×12×18	H540×200×12×18	□650×650×20	H250×250×10×16
4	H530×240×10×16	H530×240×10×16	H560×200×12×18	H560×200×12×18	□750×750×25	H250×250×10×16
3	H530×250×10×16	H530×250×10×16	H570×200×12×18	H570×200×12×18	□750×750×25	H250×250×10×16
2	H540×250×10×16	H540×250×10×16	H570×200×12×18	H570×200×12×18	□820×820×25	H250×250×10×16
1	H540×250×10×16	H540×250×10×16	H580×200×12×18	H580×200×12×18	□820×820×25	H250×250×10×16

with ordinary steel and HSS, respectively. Compared with the design cross-section, the HSS used in the frame beams and columns can significantly reduce the cost of the non-energy dissipation members. However, the link sections of HK structures are marginally greater than those on OK models. The fundamental period of the structure is estimated by the PBSD method, and the period of the HK buildings is greater than OK because of its small column section. The base shear of the HK structure is also greater than for the OK frames. In the 15-story buildings, the member section for *X*-direction is the same with the *Y*-

Table 8 Member sections of HK-S15

Story	Beams in *X*-direction	Beams in *Y*-direction	Links in *X*-direction	Links in *Y*-direction	Column	Brace
15	H270×100×6×12	H270×100×6×12	H260×140×6×12	H260×140×6×12	□200×200×10	H180×180×10×16
14	H320×150×6×12	H320×150×6×12	H300×150×8×14	H300×150×8×14	□250×250×12	H180×180×10×16
13	H360×150×8×14	H360×150×8×14	H400×160×8×14	H400×160×8×14	□250×250×12	H200×200×10×16
12	H370×180×8×14	H370×180×8×14	H390×180×10×16	H390×180×10×16	□300×300×16	H200×200×10×16
11	H420×180×8×14	H420×180×8×14	H450×180×10×16	H450×180×10×16	□300×300×16	H220×220×10×16
10	H410×180×10×16	H410×180×10×16	H500×180×10×16	H500×180×10×16	□350×350×16	H220×220×10×16
9	H440×180×10×16	H440×180×10×16	H460×200×12×18	H460×200×12×18	□350×350×16	H240×240×10×16
8	H430×200×10×16	H430×200×10×16	H500×200×12×18	H500×200×12×18	□430×430×18	H250×250×10×16
7	H450×200×10×16	H450×200×10×16	H520×200×12×18	H520×200×12×18	□430×430×18	H250×250×10×16
6	H470×200×10×16	H470×200×10×16	H550×200×12×18	H550×200×12×18	□540×540×20	H250×250×10×16
5	H480×200×10×16	H480×200×10×16	H570×200×12×18	H570×200×12×18	□540×540×20	H250×250×10×16
4	H490×200×10×16	H490×200×10×16	H580×200×12×18	H580×200×12×18	□620×620×25	H250×250×10×16
3	H500×200×10×16	H500×200×10×16	H590×200×12×18	H590×200×12×18	□620×620×25	H250×250×10×16
2	H510×200×10×16	H510×200×10×16	H600×200×12×18	H600×200×12×18	□700×700×25	H250×250×10×16
1	H510×200×10×16	H510×200×10×16	H600×200×12×18	H600×200×12×18	□700×700×25	H250×250×10×16

Table 9 Member sections of OK-S20

Story	Beams in *X*-direction	Beams in *Y*-direction	Links in *X*-direction	Links in *Y*-direction	Column	Brace
20	H310×140×6×12	H330×100×6×10	H300×140×6×12	H300×140×6×12	□350×350×18	H180×180×10×16
19	H380×150×8×14	H300×150×8×14	H360×140×8×14	H300×150×8×14	□350×350×18	H200×200×10×16
18	H440×160×8×14	H370×150×8×14	H360×160×8×14	H370×160×8×14	□400×400×18	H200×200×10×16
17	H400×200×10×16	H380×180×8×14	H420×160×8×14	H440×160×8×14	□400×400×20	H220×220×10×16
16	H450×200×10×16	H400×200×8×14	H480×160×8×14	H410×180×10×16	□400×400×20	H220×220×10×16
15	H460×220×10×16	H430×200×8×14	H440×180×10×16	H450×180×10×16	□450×450×20	H220×220×12×18
14	H500×220×10×16	H410×200×10×16	H470×180×10×16	H490×180×10×16	□450×450×20	H220×220×12×18
13	H520×220×10×16	H440×200×10×16	H510×180×10×16	H520×180×10×16	□500×500×20	H230×230×12×18
12	H550×220×10×16	H460×200×10×16	H530×180×10×16	H550×180×10×16	□500×500×20	H230×230×12×18
11	H500×240×12×18	H480×200×10×16	H570×180×10×16	H580×180×10×16	□550×550×22	H230×230×12×18
10	H510×240×12×18	H500×200×10×16	H510×200×12×18	H520×200×12×18	□550×550×22	H240×240×12×18
9	H530×240×12×18	H510×200×10×16	H530×200×12×18	H540×200×12×18	□600×600×22	H240×240×12×18
8	H540×240×12×18	H520×200×10×16	H540×200×12×18	H550×200×12×18	□600×600×22	H250×250×12×18
7	H540×250×12×18	H540×200×10×16	H560×200×12×18	H570×200×12×18	□600×600×25	H250×250×12×18
6	H550×250×12×18	H550×200×10×16	H570×200×12×18	H580×200×12×18	□650×650×25	H250×250×12×18
5	H560×250×12×18	H510×200×12×18	H580×200×12×18	H600×200×12×18	□700×700×25	H250×250×12×18
4	H570×250×12×18	H520×200×12×18	H590×200×12×18	H620×200×12×18	□800×800×30	H280×280×14×20
3	H580×250×12×18	H530×200×12×18	H600×200×12×18	H630×200×12×18	□880×880×30	H280×280×14×20
2	H590×250×12×18	H530×200×12×18	H610×200×12×18	H640×200×12×18	□970×970×32	H280×280×14×20
1	H590×250×12×18	H540×200×12×18	H610×200×12×18	H650×200×12×18	□970×970×32	H280×280×14×20

Table 10 Member sections of HK-S20

Story	Beams in *X*-direction	Beams in *Y*-direction	Links in *X*-direction	Links in *Y*-direction	Column	Brace
20	H300×110×6×12	H300×100×6×12	H300×140×6×12	H300×140×6×12	□300×300×18	H180×180×10×16
19	H310×150×8×14	H310×100×8×14	H300×160×8×14	H300×150×8×14	□300×300×18	H200×200×10×16
18	H380×150×8×14	H310×150×8×14	H370×160×8×14	H380×160×8×14	□350×350×18	H200×200×10×16
17	H370×170×10×16	H320×150×10×16	H360×180×10×16	H450×160×8×14	□350×350×20	H220×220×10×16
16	H400×180×10×16	H340×160×10×16	H410×180×10×16	H420×180×10×16	□350×350×20	H220×220×10×16
15	H430×180×10×16	H350×170×10×16	H460×180×10×16	H470×180×10×16	□400×400×20	H220×220×12×18
14	H430×200×10×16	H380×170×10×16	H500×180×10×16	H510×180×10×16	□400×400×20	H220×220×12×18
13	H460×200×10×16	H400×170×10×16	H530×180×10×16	H540×180×10×16	□400×400×20	H230×230×12×18
12	H480×200×10×16	H420×170×10×16	H480×200×12×18	H490×200×12×18	□450×450×20	H230×230×12×18
11	H460×200×12×18	H400×170×12×18	H500×200×12×18	H520×200×12×18	□450×450×22	H230×230×12×18
10	H470×200×12×18	H400×180×12×18	H530×200×12×18	H540×200×12×18	□450×450×22	H240×240×12×18
9	H490×200×12×18	H410×180×12×18	H550×200×12×18	H560×200×12×18	□500×500×22	H240×240×12×18
8	H500×200×12×18	H420×180×12×18	H560×200×12×18	H580×200×12×18	□500×500×22	H250×250×12×18
7	H510×200×12×18	H430×180×12×18	H580×200×12×18	H590×200×12×18	□500×500×25	H250×250×12×18
6	H520×200×12×18	H440×180×12×18	H590×200×12×18	H610×200×12×18	□550×550×25	H250×250×12×18
5	H530×200×12×18	H450×180×12×18	H600×200×12×18	H620×200×12×18	□550×550×25	H250×250×12×18
4	H540×200×12×18	H460×180×12×18	H620×200×12×18	H650×200×12×18	□650×650×30	H280×280×14×20
3	H540×200×12×18	H470×180×12×18	H620×200×12×18	H660×200×12×18	□700×700×30	H280×280×14×20
2	H550×200×12×18	H470×180×12×18	H630×200×12×18	H660×200×12×18	□770×770×30	H280×280×14×20
1	H550×200×12×18	H480×180×12×18	H630×200×12×18	H670×200×12×18	□770×770×30	H280×280×14×20

direction, which is identical with the plan design. Therefore, the results of nonlinear static analysis and dynamic analysis are the same as well.

3.4 Dynamic property

The first three periods of the structures are obtained by modal analysis as list in Table 11. High-strength steel is used in the frame columns to reduce the section sizes of the members and weaken the stiffness of the structure, resulting in the lateral stiffness of *K*-EBFs with HSS being smaller than for the OK structure, and its fundamental period increases with increasing structural stories. The differences in periods of same-height structures increases with increasing height, that is consistent with the trend of greater differences between the design sections of frame columns.

3.5 Result of nonlinear static analysis

The analysis models of the structures were developed in SAP2000. All links are shear yielding, and the cross-section along the length of the links reaches the yielding state. The shear hinges are specified at the two ends and the middle of the links, and the bending hinges are specified at the two ends of the non-energy dissipation beams. The P-M hinges are then specified at either ends of the column, and the horizontal loading is distributed in inverted triangle mode to push the structure to the ultimate state. The curve of the relationship between the base shear and the roof drift ratio is defined as the pushover curve, and the structures enter the ultimate state when the plastic hinge deformation is increased to the maximum, the corresponding bearing capacity is known as the ultimate base shear. The pushover curves and yield of ductile members obtained from nonlinear static analyses for four prototypes are displayed in Fig. 15.

Table 11 Fundamental structure periods

Example	T_1/s	T_2/s	T_3/s
OK-S5	0.591	0.230	0.138
HK-S5	0.605	0.237	0.145
OK-S10	1.016	0.367	0.210
HK-S10	1.107	0.396	0.223
OK-S15	1.495	0.525	0.288
HK-S15	1.629	0.563	0.305
OK-S20	2.159	0.733	0.386
HK-S20	2.419	0.793	0.409

As observed from the figures, the elastic end points of the pushover curves are defined as yielding point, and the end points of the pushover curves are defined as ultimate point. The corresponding bearing capacity and roof drift of yielding point and ultimate point are list in Table 12, the lateral stiffness is equal to bearing capacity divided by roof displacement of yielding point, and the ductility is equal to the ratio of the ultimate roof drift to yield roof drift. The lateral stiffness of HK structures is a little lower than the OK due to the high strength steel reduced the cross-section of the columns. The ductility ratio of HK is lower than the OK models, which is identical with the theoretical calculation of the yielding drift and ultimate drift in PBSD method.

The plastic hinges in SAP2000 models are the rigid-plastic and no elastic behavior in the hinges, so there is a hinge unloading phenomenon when the deformation of the plastic hinges reach to the maximum, and the lateral stiffness of the structure suddenly drops. The corresponding point in the pushover curves is ultimate state, and then the pushover curves are cliff falling over the ultimate state because of the hinges unloading. The bearing capacity for the HK buildings in the yielding state is approximately with OK buildings because of the links is designed closed to each other.

Story drift and link rotation for four group prototypes are list in Tables 13-16, and the story drift in yielding state distribution along the height of the structure are comparison as depicted in Fig. 16. As recommended by FEM356, the "Collapse prevention limit" for story drift is 2% and the elastic story drift limit is 0.4%, and the link plastic rotation (the link rotation in ultimate state minus the link rotation in yielding state) limit is 0.08 rad according to AISC341-10. The story drift for bottom structures are the lowest for all prototypes on account of the first story stiffness is greatest,

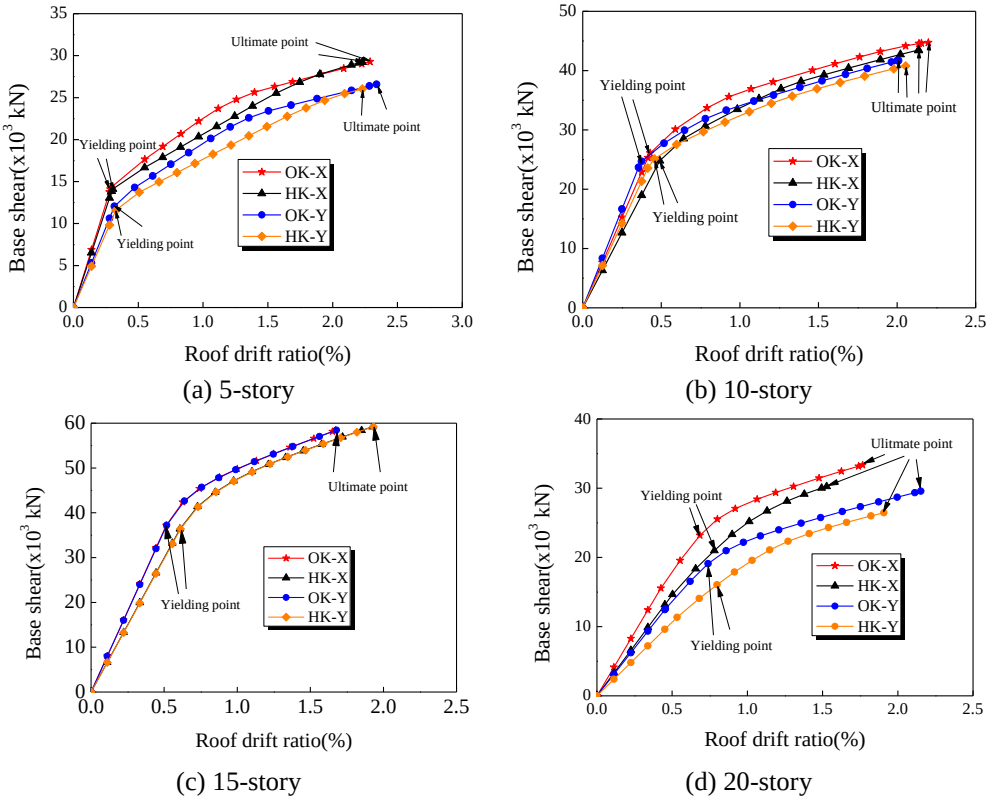

(a) 5-story (b) 10-story

(c) 15-story (d) 20-story

Fig. 15 Pushover curves

Table 12 Performance data of models in pushover curves

Model		Yielding point				Ultimate point				Lateral stiffness/ kN·mm		Ductility	
		Bearing/×10^{3}kN		Roof drift/%		Bearing/×10^{3}kN		Roof drift/%					
		OK	HK	OK	HK	OK	HK	OK	HK	OK	HK	OK	HK
5-story	*X*	14.32	14.12	0.29	0.30	29.34	29.23	2.30	2.23	275.1	261.2	7.91	7.35
	Y	12.06	11.60	0.32	0.33	26.59	26.15	2.34	2.28	212.2	196.5	7.40	6.97
10-story	*X*	25.30	24.81	0.41	0.49	44.71	43.39	2.20	2.14	169.5	140.7	5.31	4.36
	Y	23.68	23.56	0.36	0.41	41.69	40.79	2.01	2.05	185.2	158.2	5.66	4.96
15-story	*X*	37.22	36.39	0.51	0.61	58.41	59.20	1.67	1.93	146.2	120.8	3.25	3.16
	Y	37.22	36.39	0.52	0.61	58.45	59.23	1.68	1.93	145.3	120.2	3.25	3.16
20-story	*X*	15.56	14.64	0.43	0.50	33.35	30.26	1.77	1.53	51.7	41.1	4.16	3.04
	Y	12.56	11.35	0.46	0.53	29.58	26.12	2.15	1.91	38.9	30.1	4.72	3.58

Table 13 Story drift and link rotation for 5-story

story	Story drift/%								Link rotation/rad							
	Yielding point				Ultimate point				Yielding point				Ultimate point			
	OK-X	OK-Y	HK-X	HK-Y	OK-X	OK-Y	HK-X	HK-Y	OK-X	OK-Y	HK-X	HK-Y	OK-X	OK-Y	HK-X	HK-Y
1	0.22	0.24	0.23	0.24	2.07	2.05	1.58	1.58	0.006	0.005	0.006	0.004	0.131	0.127	0.098	0.095
2	0.31	0.34	0.32	0.35	2.65	2.70	2.48	2.58	0.008	0.006	0.008	0.005	0.166	0.164	0.155	0.157
3	0.31	0.35	0.32	0.35	2.70	2.76	2.70	2.84	0.007	0.006	0.007	0.005	0.169	0.168	0.170	0.174
4	0.31	0.34	0.32	0.36	2.34	2.39	2.46	2.55	0.008	0.007	0.008	0.006	0.146	0.143	0.155	0.155
5	0.28	0.32	0.30	0.34	1.73	1.79	1.89	1.86	0.009	0.008	0.009	0.008	0.107	0.105	0.119	0.111

with the corresponding to avoid weak story in PBSD method. In the yielding state, the story drifts and link rotations are uniformly distribution along the height structure, accord with the prediction of PBSD method. In the ultimate state, the story drifts in the inner height of the structure are larger than 2%, and the link plastic rotations are over 0.08 rad as well, therefore, all models have excellent deformation capacity.

Failure modes for all prototypes in the ultimate state from the pushover analysis are displayed in Figs. 17-20. As observed in this figure, in all four prototypes structures designed by the PBSD method, all link members yield first as the “energy dissipation fuses”, and then the flexural beams enter the inelastic phase and undergo the permanent

Table 14 Story drift and link rotation for 10-story

story	Story drift/%								Link rotation/rad							
	Yielding point				Ultimate point				Yielding point				Ultimate point			
	OK-X	OK-Y	HK-X	HK-Y	OK-X	OK-Y	HK-X	HK-Y	OK-X	OK-Y	HK-X	HK-Y	OK-X	OK-Y	HK-X	HK-Y
1	0.21	0.18	0.24	0.23	0.99	0.71	0.96	0.89	0.004	0.004	0.004	0.005	0.055	0.038	0.052	0.050
2	0.36	0.32	0.38	0.41	1.84	1.57	1.92	1.85	0.005	0.006	0.004	0.010	0.104	0.065	0.108	0.108
3	0.42	0.37	0.44	0.46	2.42	2.18	2.49	2.41	0.006	0.007	0.004	0.010	0.141	0.130	0.142	0.142
4	0.44	0.39	0.48	0.46	2.76	2.55	2.71	2.63	0.004	0.006	0.003	0.006	0.161	0.152	0.152	0.152
5	0.47	0.41	0.53	0.48	2.97	2.76	2.91	2.78	0.005	0.006	0.003	0.005	0.175	0.165	0.163	0.160
6	0.48	0.42	0.55	0.49	2.88	2.71	2.72	2.63	0.004	0.005	0.002	0.004	0.165	0.159	0.145	0.146
7	0.50	0.43	0.58	0.52	2.68	2.54	2.49	2.41	0.004	0.005	0.003	0.004	0.149	0.146	0.128	0.128
8	0.48	0.42	0.57	0.52	2.27	2.16	2.08	2.03	0.004	0.005	0.002	0.004	0.123	0.120	0.101	0.103
9	0.50	0.43	0.59	0.52	1.85	1.72	1.76	1.70	0.006	0.005	0.004	0.004	0.094	0.071	0.078	0.080
10	0.44	0.37	0.53	0.47	1.34	1.19	1.31	1.22	0.005	0.004	0.003	0.003	0.063	0.055	0.051	0.049

Table 15 Story drift and link rotation for 15-story

story	Story drift/%				Link rotation/rad			
	Yielding point		Ultimate point		Yielding point		Ultimate point	
	OK-X	HK-X	OK-X	HK-X	OK-X	HK-X	OK-X	HK-X
1	0.18	0.20	0.48	0.57	0.003	0.003	0.018	0.024
2	0.34	0.36	1.09	1.28	0.004	0.004	0.050	0.060
3	0.40	0.44	1.54	1.76	0.004	0.003	0.073	0.084
4	0.44	0.48	1.84	2.05	0.003	0.003	0.087	0.096
5	0.48	0.53	2.10	2.27	0.003	0.002	0.100	0.099
6	0.51	0.57	2.24	2.33	0.002	0.001	0.103	0.102
7	0.55	0.63	2.33	2.43	0.002	0.001	0.105	0.109
8	0.56	0.66	2.29	2.33	0.002	0.000	0.099	0.102
9	0.60	0.71	2.26	2.38	0.001	0.000	0.093	0.091
10	0.61	0.73	2.07	2.20	0.001	0.001	0.079	0.075
11	0.63	0.76	1.91	2.14	0.001	0.001	0.067	0.069
12	0.62	0.76	1.56	1.88	0.000	0.001	0.043	0.051
13	0.63	0.78	1.33	1.97	0.000	0.001	0.027	0.057
14	0.62	0.77	1.18	1.69	0.001	0.000	0.020	0.041
15	0.56	0.74	0.86	1.61	0.000	0.000	0.002	0.039

Table 16 Story drift and link rotation for 20-story

story	Story drift/%								Link rotation/rad							
	Yielding point				Ultimate point				Yielding point				Ultimate point			
	OK-X	OK-Y	HK-X	HK-Y	OK-X	OK-Y	HK-X	HK-Y	OK-X	OK-Y	HK-X	HK-Y	OK-X	OK-Y	HK-X	HK-Y
1	0.13	0.13	0.16	0.16	0.54	0.58	0.67	0.72	0.002	0.002	0.003	0.002	0.034	0.031	0.046	0.042
2	0.26	0.28	0.30	0.32	1.32	1.42	1.57	1.71	0.003	0.003	0.003	0.003	0.093	0.083	0.112	0.103
3	0.32	0.36	0.36	0.40	1.91	2.09	2.13	2.39	0.003	0.003	0.003	0.003	0.136	0.125	0.150	0.142
4	0.36	0.40	0.41	0.44	2.29	2.57	2.34	2.75	0.003	0.003	0.002	0.002	0.162	0.152	0.157	0.164
5	0.37	0.41	0.42	0.46	2.39	2.79	2.15	2.66	0.001	0.001	0.000	0.000	0.159	0.158	0.129	0.139
6	0.38	0.42	0.44	0.48	2.40	2.90	1.91	2.47	0.001	0.001	0.000	0.001	0.153	0.159	0.100	0.117
7	0.41	0.44	0.48	0.52	2.38	2.96	1.78	2.37	0.000	0.000	0.001	0.001	0.145	0.156	0.081	0.102
8	0.44	0.47	0.51	0.55	2.34	2.96	1.66	2.26	0.000	0.000	0.001	0.001	0.136	0.150	0.064	0.087
9	0.45	0.49	0.54	0.58	2.38	2.90	1.56	2.14	0.000	0.001	0.002	0.002	0.124	0.138	0.047	0.071
10	0.48	0.51	0.57	0.61	2.22	2.83	1.52	2.07	0.001	0.001	0.002	0.002	0.114	0.128	0.038	0.060
11	0.49	0.52	0.59	0.62	2.12	2.72	1.44	1.95	0.001	0.001	0.002	0.003	0.100	0.115	0.026	0.046
12	0.51	0.54	0.60	0.63	2.04	2.62	1.38	1.87	0.001	0.001	0.003	0.003	0.091	0.104	0.017	0.036
13	0.51	0.55	0.62	0.65	1.89	2.44	1.39	1.86	0.002	0.002	0.003	0.003	0.074	0.087	0.014	0.031
14	0.52	0.56	0.62	0.66	1.77	2.28	1.33	1.76	0.001	0.002	0.003	0.003	0.062	0.073	0.005	0.021
15	0.52	0.56	0.62	0.66	1.60	2.06	1.27	1.66	0.002	0.002	0.003	0.003	0.045	0.055	0.001	0.012
16	0.53	0.57	0.64	0.67	1.49	1.89	1.30	1.66	0.002	0.002	0.003	0.003	0.034	0.040	0.001	0.010
17	0.53	0.56	0.63	0.66	1.33	1.67	1.26	1.55	0.002	0.002	0.003	0.003	0.020	0.024	0.004	0.002
18	0.52	0.55	0.62	0.65	1.19	1.50	1.24	1.45	0.002	0.002	0.003	0.004	0.008	0.012	0.005	0.005
19	0.51	0.55	0.63	0.65	1.14	1.39	1.25	1.42	0.001	0.001	0.002	0.003	0.006	0.005	0.003	0.005
20	0.47	0.49	0.58	0.57	0.99	1.15	1.15	1.24	0.002	0.003	0.004	0.005	0.004	0.007	0.007	0.011

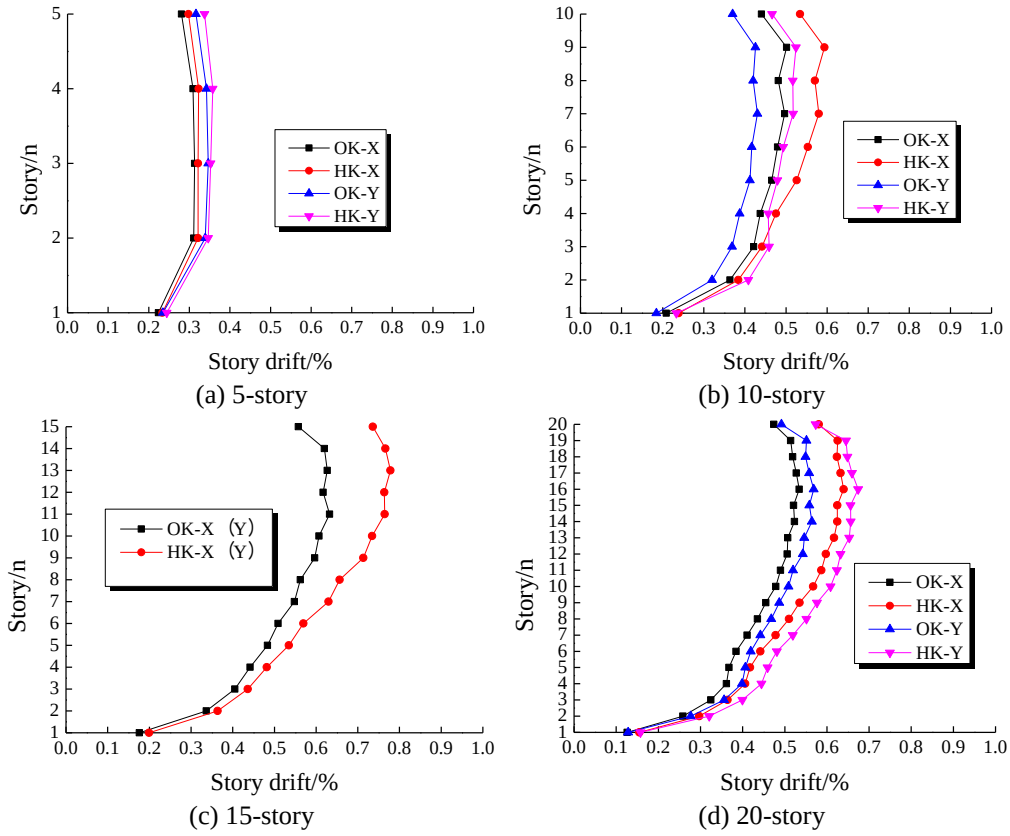

Fig. 16 Story drifts distribution

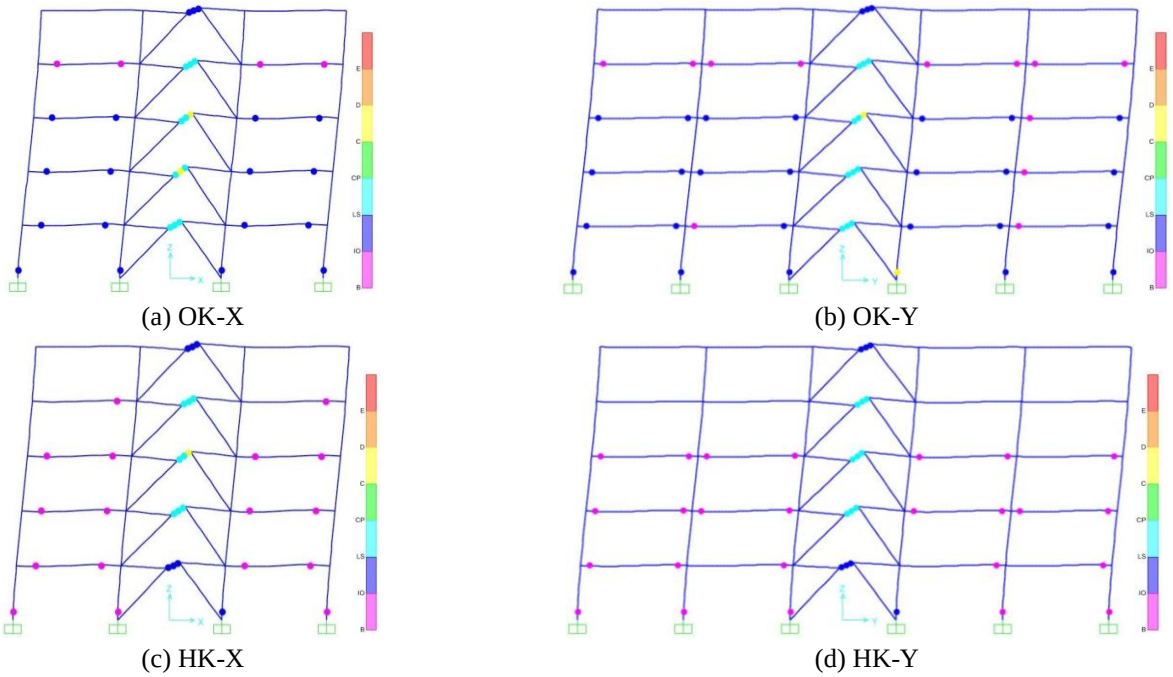

Fig. 17 Failure mode for 5-story building

deformations as the "multiple seismic fortification", and the last, the column bases are yielding to the ultimate state of the structures. Considering the order of yield in members, the yield mechanism of the structure is obtained as well. As seen in the failure modes, the links for each story are yielding to dissipate seismic energy, the braces and the columns except the first story are remain in elastic, the failure modes are closed to the desired damage predicted by the PBSD method, and the yielding mechanisms of all structures are identical with the story drift and link rotation distribution. In the HK compared with OK prototypes, the plastic development level is decreased with the high

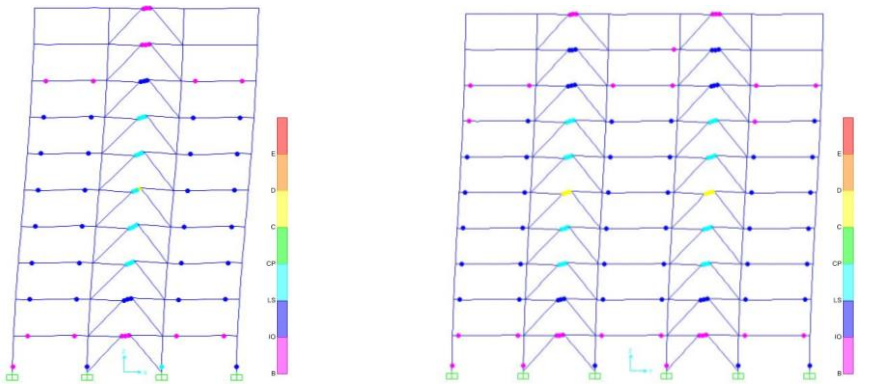

(a) OK-X (b) OK-Y

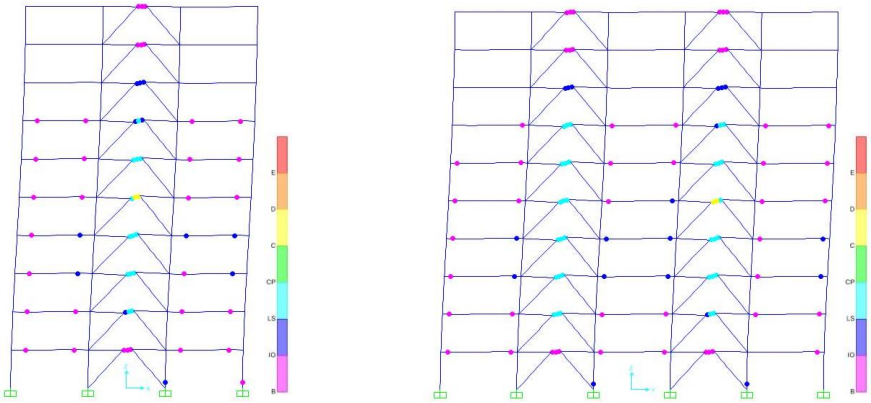

(c) HK-X (d) HK-Y

Fig. 18 Failure mode for 10-story building

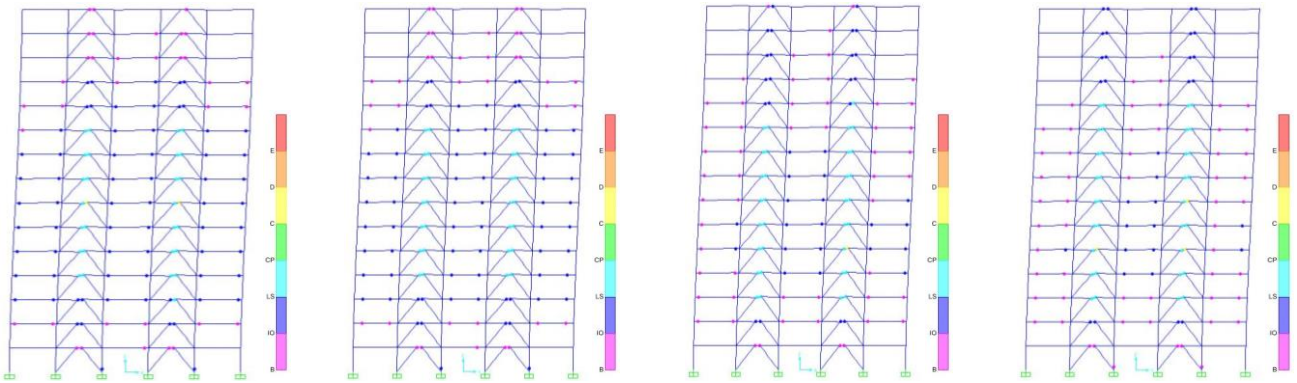

(a) OK-X (b) OK-Y (c) HK-X (d) HK-Y

Fig. 19 Failure mode for 15-story building

strength steel used in moment beams.

3.6 Ground motion record

The dynamic analysis was conducted using a set of ground motions which recommended in FEMA695. The seismological properties of the ground motions are summarized in Table 17 include the numbers of ground motions, seismic events, occurrence times, recording stations, the magnitude *M*, the closest distance to the fault *R*, the maximum acceleration PGA (g), and the maximum velocity PGV (cm/s). The spectral characteristics, duration, maximum acceleration, recording point, and pulse effect of each ground motion record are different. Therefore, the above suite of strong motions covers well-defined design scenarios. All prototypes were subjected to nonlinear dynamic analysis with various ground motions. A 2% probability of exceedance in a 50-year period was used as the rare earthquake level of seismic hazard. The acceleration response spectra of the ensemble of accelerograms, along with the design acceleration spectrum are shown in Fig. 21.

3.7 Results of nonlinear dynamic analysis

3.7.1 Failure mode

The failure modes of all buildings in the hazard level with exceedance probability of 2% in 50 years (rare

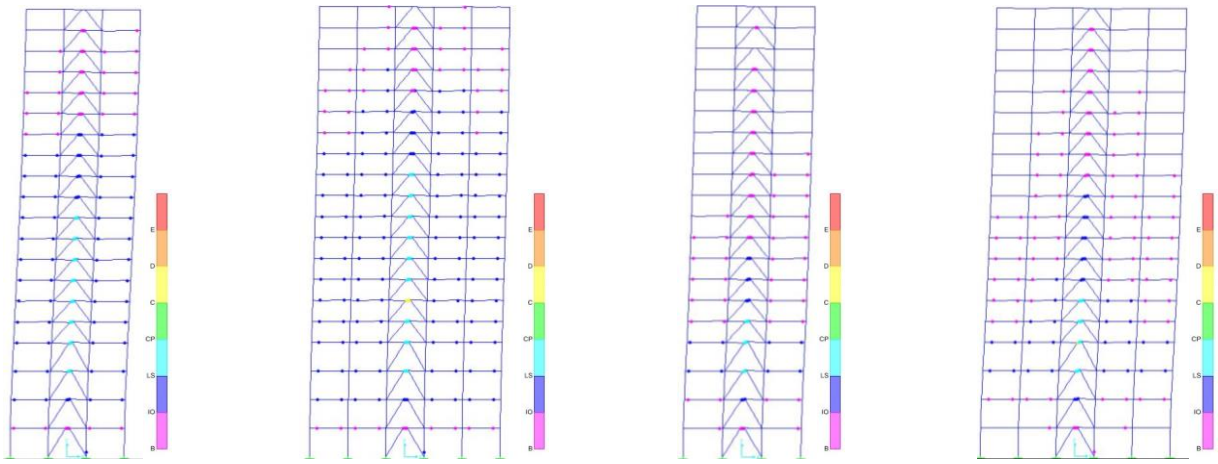

(a) OK-X (b) OK-Y (c) HK-X (d) HK-Y

Fig. 20 Failure mode for 20-story building

Table 17 Ground motion records

Number	Seismic record	Seismic event	Recording station	*M*	*R*/km	*PGA*/g	*PGV*/(cm/s)
1	NGA0829	Cape Mendocino 1992/04/25 18:06	89324 Rio Dell Overpass - FF	7.0	14.30	0.549	42.1
2	NGA0727	Superstitn Hills(B) 1987/11/24 13:16	01335 El Centro Imp. Co. Cent	6.5	5.60	0.894	42.2
3	NGA0802	Loma Prieta 1989/10/18 00:05	58065 Saratoga - Aloha Ave	6.9	13.0	0.324	41.2
4	NGA1485	Chi-Chi, Taiwan 1999/09/20	TCU045	7.6	24.1	0.512	39.0
5	NGA0068	San Fernando 1971/02/09 14:00	135 LA - Hollywood Stor Lot	6.6	21.2	0.210	18.9
6	NGA0821	Erzincan, Turkey 1992/03/13	95 Erzincan	6.9	2.0	0.496	64.3
7	NGA1605	Duzce, Turkey 1999/11/12	Duzce	7.1	8.2	0.535	83.5
8	NGA0292	Irpinia, Italy 1980/11/23 19:34	Sturno	6.5	32.0	0.358	52.7
9	NGA0181	Imperial Valley 1979/10/15 23:16	942 El Centro Array #6	6.5	1.0	0.439	109.8
10	NGA0960	Northridge 1994/01/17 12:31	90057 Canyon Country - W Lost Cany	6.7	13.0	0.482	45.1

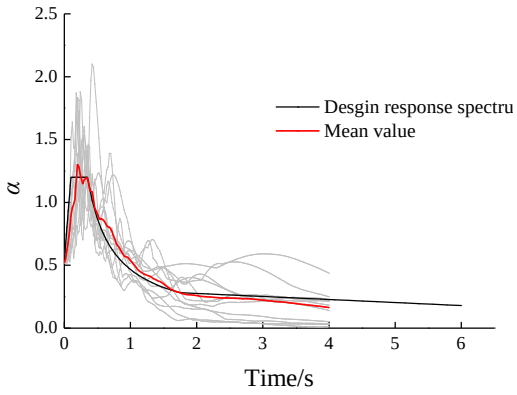

Fig. 21 Design spectra and scaled earthquake spectra

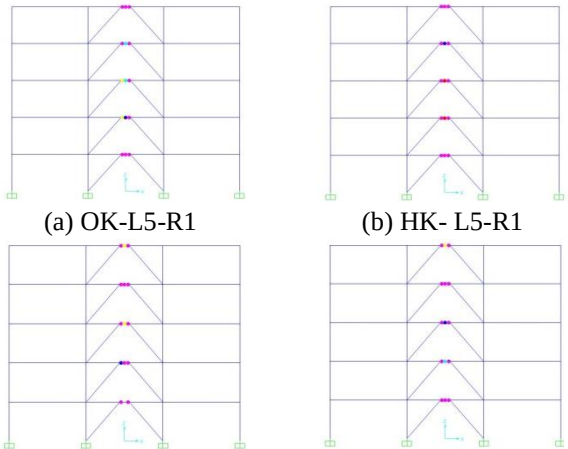

(a) OK-L5-R1 (b) HK- L5-R1

(c) OK-L5-R2 (d) HK-L5-R2

Fig. 22 Failure mode for 5-story building under rare earthquake

earthquake) are shown in Figs. 22-25. In the graphs, the R1 and R2 represent of seismic record NGA0829 and NGA0727, respectively. The failure modes show that links are primarily involved to dissipate energy, and the braces and columns are remain in elastic. The failure modes of HK structures are similar with the OK structures. In 5-story and 10-story buildings, all links yielding with other members still in elastic, while in 15-story and 20-story models, a few beam flexural yielding to dissipate energy due to the influence of high order mode.

The structural failure modes are the links in each story are involved in energy dissipation, and the rest of the non-energy dissipating components are mainly in the elastic state with identical with story drift is uniformly along the height of the structure. The failure modes are approximated to ideal damage state. The PBSD method has achieved the expected goal from the view of plastic hinge distribution. Moreover, the HK and the OK structures have similar ultimate states under rare earthquakes, and their performance states are similar, indicating that the structure designed based on the performance-based seismic design method can be comparable.

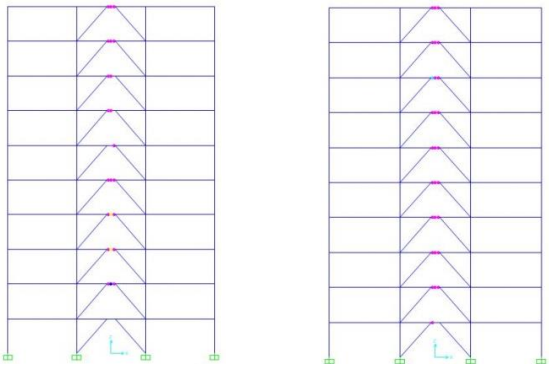

(a) OK- L10-R1 (b) HK- L10-R1

(c) OK-L10-R2 (d) HK-L10-R2

Fig. 23 Failure mode for 10-story building under rare earthquake

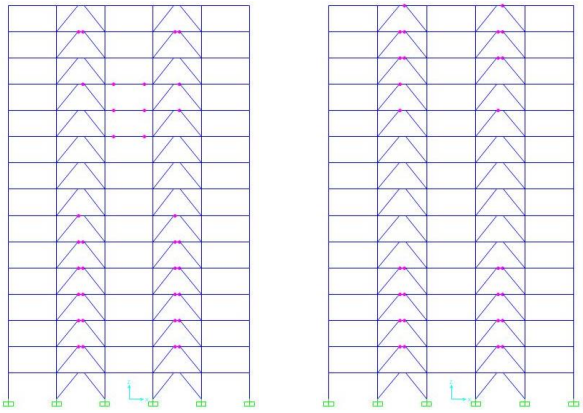

(a) OK- L15-R1 (b) HK- L15-R1

(c) OK-L15-R2 (d)HK-L15-R2

Fig. 24 Failure mode for 15-story building under rare earthquake

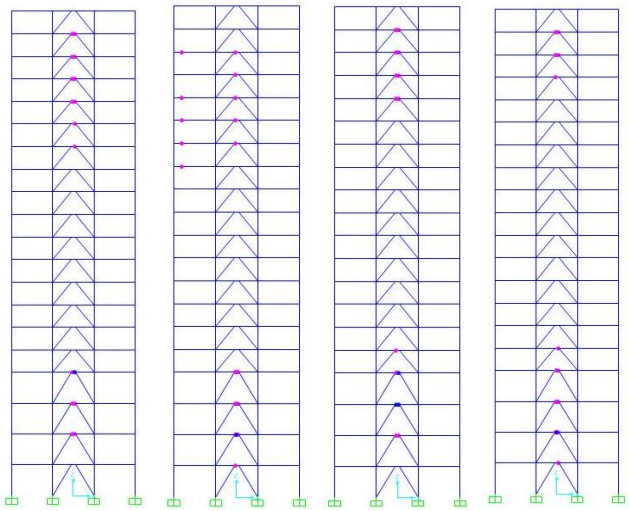

(a) OK- L20-R1 (b) HK- L20-R1 (c) OK-L20-R2 (d) HK-L20-R2

Fig. 25 Failure mode for 20-story building under rare earthquake

3.7.2 Story drift and link rotation

In Figs. 26-29, the maximum story drifts for the earthquake with the exceedance probability of 2% in 50 years are displayed for 5-story, 10-story, 15-story and 20-story prototypes, and the mean values of story drifts for HK buildings and OK buildings under rare earthquakes are compared with each other. As observed in these graphs, in the 5-story structures, the maximum of median story drifts are occurred in third floor which are 0.74% for OK model and 0.77% for HK model and its minimum in first floor is 0.35% for OK and 0.39% for HK. In the 10-story buildings and in the same hazard level, maximum of median story drift is occurred in ninth floor which are 0.76% for OK and 0.96% for HK and its minimum in first floor is 0.21% for OK and 0.25% for HK. And in the 15-story buildings and in the same hazard level, maximum of median story drift is occurred in fourteen floor which are 0.88% for OK model and 1.02% for HK model and its minimum in first floor is 0.17% for OK model and 0.19% for HK model. In the 20-story structures, and in the same hazard level, maximum of median story drift is occurred in eighteenth floors which are 0.78% for OK model and 0.88% for HK model and its minimum in first floor is 0.14% for OK model and 0.18% for HK model. The collapse prevent story drift limit for design in the hazard level of rare earthquakes is 2%, and the obtained median story drift of all structures are lower than the limit state. The story drifts distribution of OK structure is similar with the HK, and the drifts values of HK buildings are higher than or equal to the OK. The story drifts distribution along the structure height is identical with the results of the nonlinear state analysis, there the lower floors have greater story lateral stiffness and lower story drift, and the story drifts distribution is close to uniformly with the pre-selected yielding mechanism.

The link plastic rotation limit is 0.08 rad for shear yielding links according to AISC341-10. As similar with “Collapse prevent limit” for story drift, the stiffness and strength degradation will occur if the link rotation is too

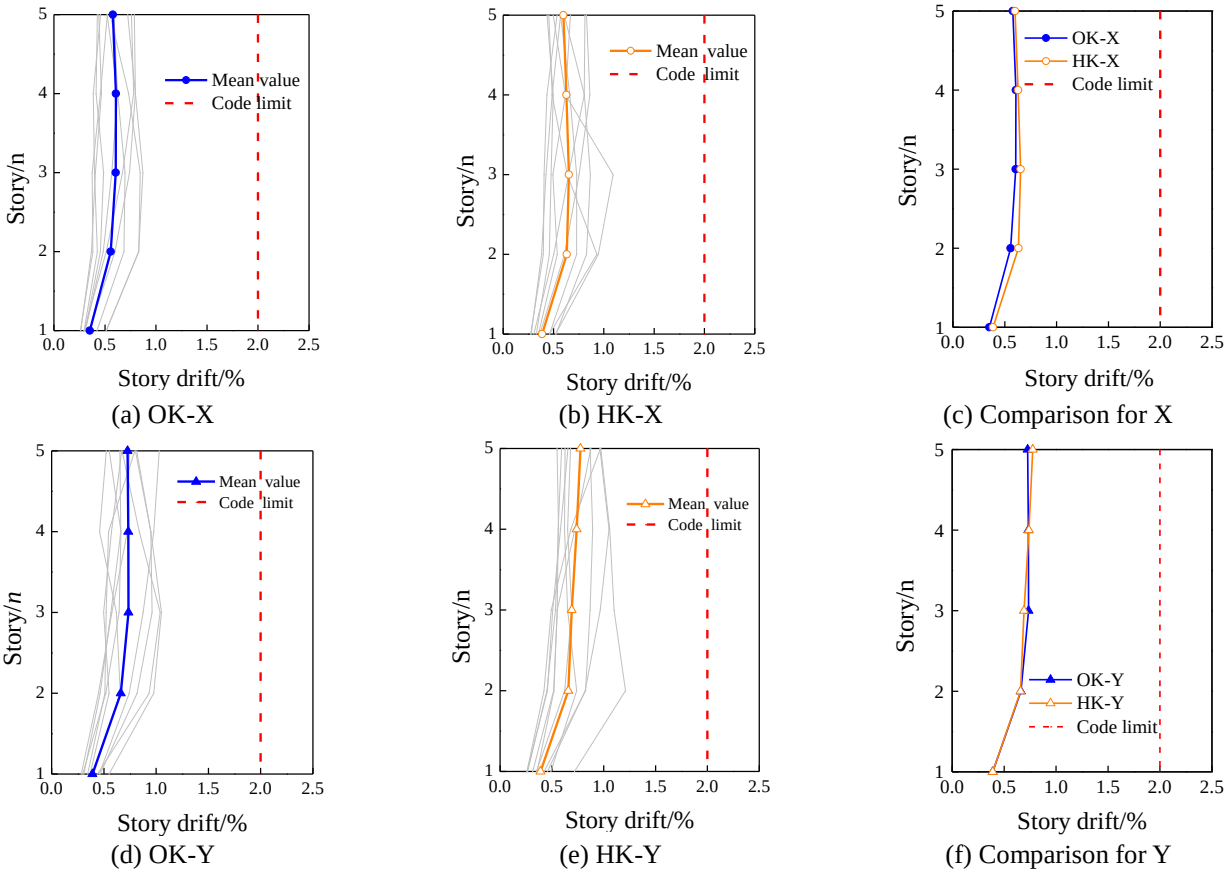

(a) OK-X (b) HK-X (c) Comparison for X

(d) OK-Y (e) HK-Y (f) Comparison for Y

Fig. 26 Story drift distribution for 5-story building under rare earthquake

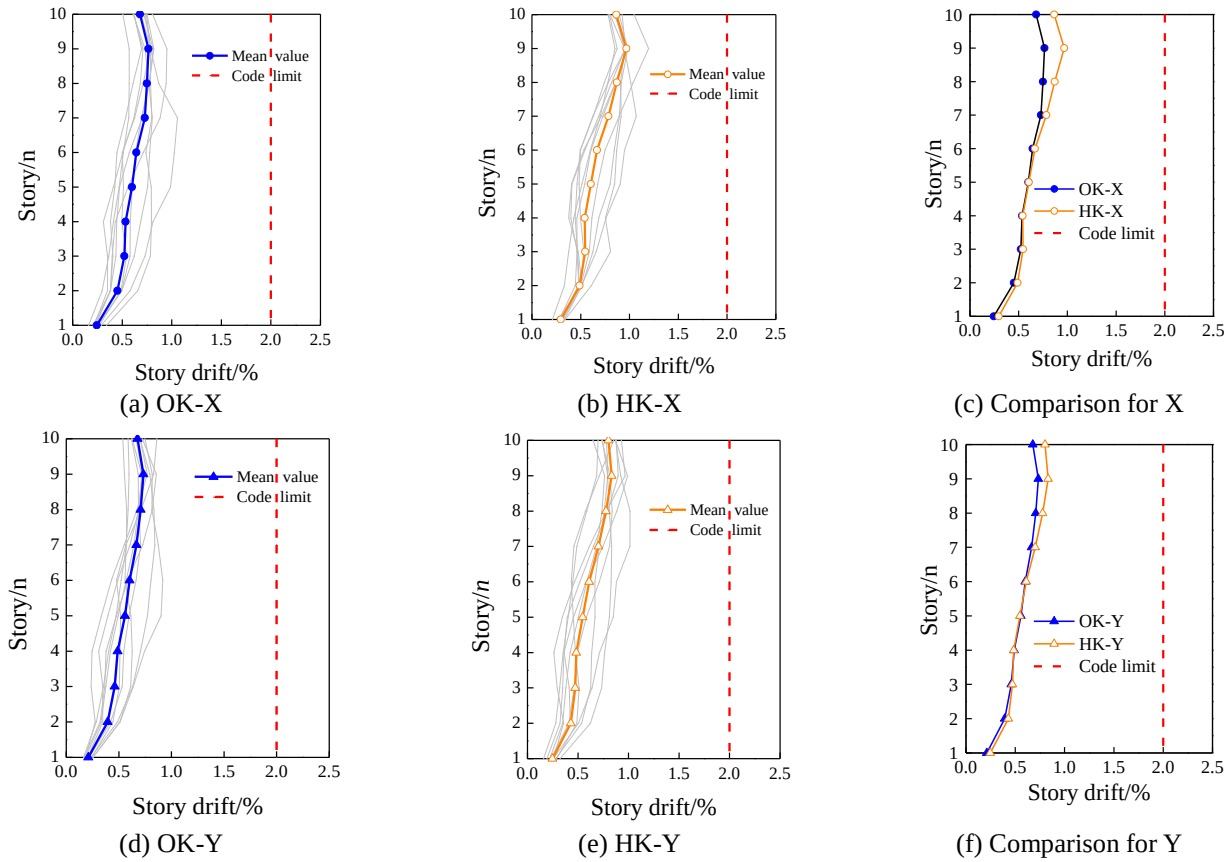

(a) OK-X (b) HK-X (c) Comparison for X

(d) OK-Y (e) HK-Y (f) Comparison for Y

Fig. 27 Story drift distribution for 10-story building under rare earthquake

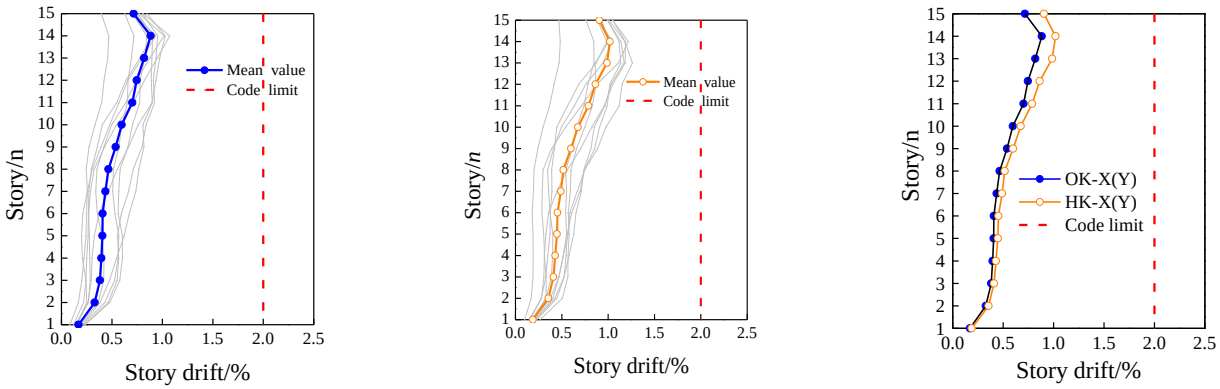

(a) OK (b) HK (c) Comparison

Fig. 28 Story drift distribution for 15-story building under rare earthquake

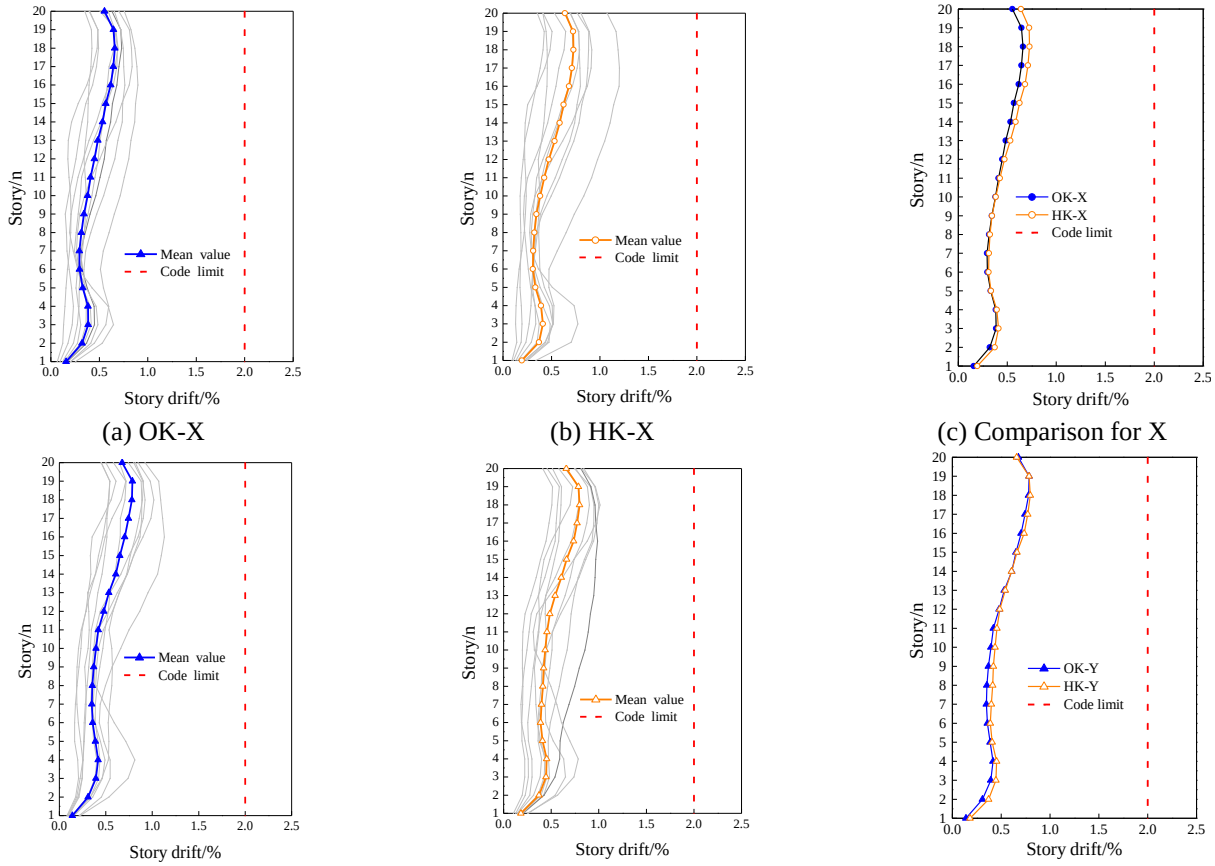

(a) OK-X (b) HK-X (c) Comparison for X

(d) OK-Y (e) HK-Y (f) Comparison for Y

Fig. 29 Story drift distribution for 20-story building under rare earthquake

large. The link rotations distribution along the structure height for 5-story, 10-story, 15-story and 20-story are depicted in Fig. 30-Fig. 33. The link rotations distribution is lower in the lower floors and equal to uniformly, and all link rotations are not greater than the code limit which in accord with the story drift distribution. In the 20-story structures, the story height for 1-4 floors is 4.5 m which is bigger than others but all link length are the same, when the story drifts occurred uniformly resulting in more story displacement and higher link rotations than other floors. The link rotations distribution is in keeping with the failure mode under rare earthquake.

4. Steel consumption

The statistical steel consumption data for members is list in Table 18. The cross-section of the links and beams with braces for HK structures are similar with the OK models which is meet with the performance pre-selected target, therefore the usage of steel in beams with braces and braces are approximately close with each other. The total steel consumption for OK and HK buildings are displayed in Fig. 34, the HY buildings of 5-story, 10-story, 15-story and 20-story respectively save 9.4%, 15.6%, 11.8%, and 13.3% less steel than OY models. The non-energy-consuming elements

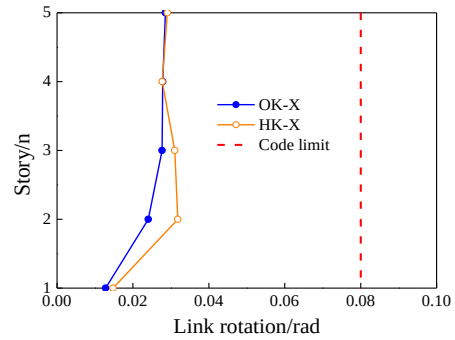

(a) *X*-direction

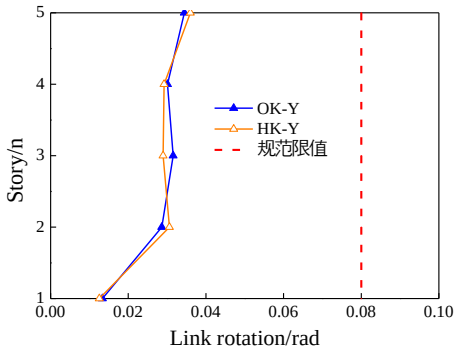

(b) *Y*-direction

Fig. 30 Link rotation distribution for 5-story building under rare earthquake

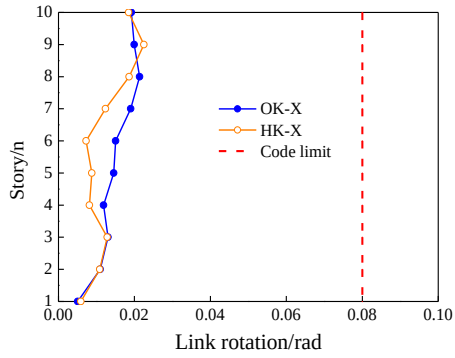

(a) *X*-direction

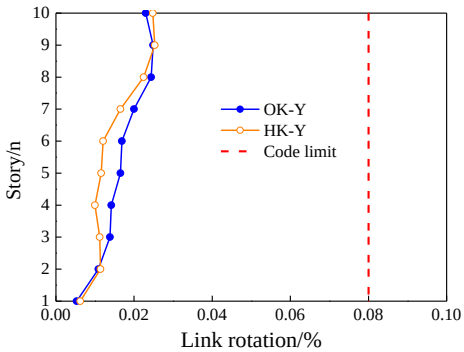

(b) *Y*-direction

Fig. 31 Link rotation distribution for 10-story building under rare earthquake

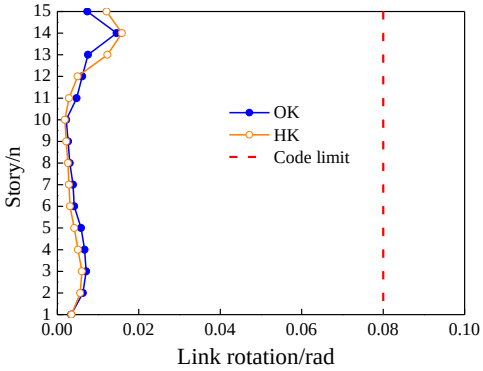

Fig. 32 Link rotation distribution for 15-story building under rare earthquake

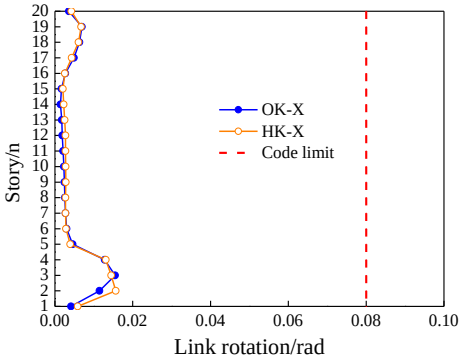

(a) *X*-direction

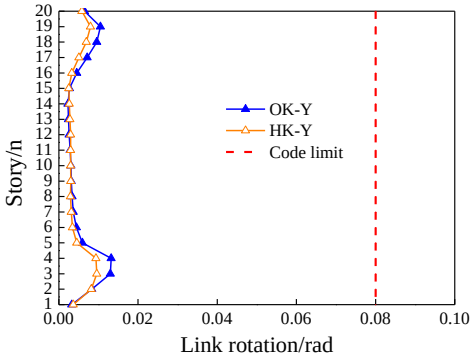

(b) *Y*-direction

Fig. 33 Link rotation distribution for 20-story building under rare earthquake

Table 18 Statistical tables for steel consumption (t in unit)

Building		Columns	Beams with no braces	Beams with braces	Braces
5-story	OK	94.8	74.4	23.3	39.9
	HK	83.7	63.0	23.5	39.9
10-story	OK	317.7	177.5	82.6	123.8
	HK	230.1	150.0	85.6	123.8
15-story	OK	601.3	275.6	165.4	225.6
	HK	481.6	239.6	168.5	225.6
20-story	OK	797.1	305.0	96.1	151.2
	HK	639.6	275.3	100.2	151.2

used high-strength steel Q460 can save steel more than or equal to 10% compared with ordinary steel Q345. The use of high strength steel can efficiently reduce the steel cost and reduces the costs of welding, manufacturing, processing, and anti-fire and corrosion protection coatings at the same time. Moreover, the high strength steel can be

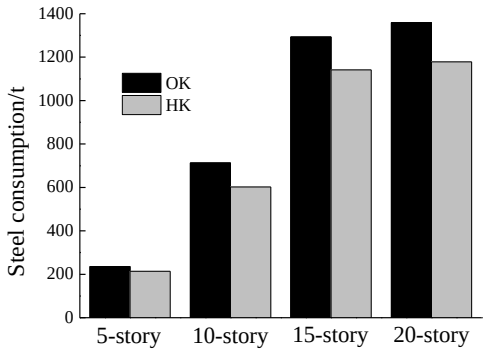

Fig. 34 Total steel consumption

used in seismic fortification structure, and the decrease of frame column can increase the area of the structure, and the economic benefit is remarkable.

5. Conclusions

Based on previous experimental study for *K*-type eccentrically braced steel frames with high-strength steel, the finite element analysis is validated by the test results. A comparative example of *K*-type eccentrically braced steel frames with high-strength steel and *K*-type eccentrically braced frames with ordinary steel is designed by performance-based seismic design method, which includes 5-story, 10-story, 15-story, and 20-story. Pushover analysis and nonlinear dynamic analysis were conducted to all models. The seismic performance and failure mode under rare earthquake between them are similar. The following results are obtained:

- The *K*-type eccentrically braced steel frames with high-strength steel structures have lower lateral stiffness and ductility than the *K*-type eccentrically braced steel frames with ordinary steel, but they have similar bearing capacity in yielding state and closely failure mode in keeping with the pre-selected performance target, which is all links yield and beams flexural yielding, and the column bases enter inelastic to performance ultimate state.
- *K*-type eccentrically braced steel frames with high-strength steel and *K*-type eccentrically braced steel frames with ordinary steel have the same performance objectives. The links of each story take part in energy dissipation, and the story drift distributes uniformly along the height, and the rest of the members are primarily in the elastic state under rare earthquake. The predicted goal of the performance-based design method is met.
- The story drifts distribution of *K*-type eccentrically braced steel frames with high-strength steel is consistent with eccentrically braced steel frames, and the high strength steel model has larger lateral story under rare earthquake.
- *K*-type eccentrically braced steel frames with high-strength steel save more than or equal to 10% steel compared with ordinary steel and reduce the cost of processing and manufacturing supporting materials, which has excellent economic benefit. Eccentrically braced steel frames with high strength steel solve the application of high strength steel in seismic fortification zone, which is helpful to popularize the extensive use of high strength steel.

Acknowledgments

The authors are grateful for the financial support received from the National Natural Science Foundation of China (Grant No. 51508463) and Special project of the science research program of the education department of Shaanxi province (Grant No. 17JK0542) and The project supported by China Postdoctoral Science Foundation (No.2017M613174), and The project supported by Natural Science Basic Research Plan in Shaanxi Province of China(Program No. 2018JQ5056) and supported By Young Talent fund of University Association for Science and Technology in Shaanxi, China (No.20170513).

References

AISC341-10 (2010), Seismic Provision for Structure Steel Buildings, American Institute of Steel Construction, Chicago, USA.

Azad, S.K. and Topkaya, C. (2017), "A review of research on steel eccentrically braced frames", *J. Constr. Steel Res.*, **128**(1), 53-73.

Bosco, M. and Rossi, P.P. (2009), "Seismic behaviour of eccentrically braced frames", *Eng. Struct.*, **31**(3), 664-674.

Dubina, D., Stratan, A., Vulcu, C. and Ciutina, A. (2015), "High strength steel in seismic resistant building frames", *Steel Constr.*, **7**(3), 173-177.

Engelhardt, M.D. and Popov, E.P. (2016), "Experimental performance of long links in eccentrically braced frames", *J. Struct. Eng.*, **118**(11), 3067-3088.

FEMA356 (2000), Prestandard and Commentary for the Seismic Rehabilitation of Buildings, Federal Emergency Management Agency, Washington, DC. USA.

FEMA695 (2009), Quantification of Building Seismic Performance Factors, Federal Emergency Management Agency, California, USA.

Fujimoto, M., Aoyagi, T., Ukai, K., Wada, A. and Saito, K. (1972), "Structural characteristics of eccentric k-braced frames", *Tran. Arch. Inst. JPN*, **195**(5), 39-49. (in Japanese)

GB50011-2010 (2010), *Code for Seismic Design of Buildings*, China Architecture Industry Press, Beijing, China. (in Chinese)

Hjelmstad, K.D. and Popov, E.P. (1983), "Cyclic behavior and design of link beams", *J. Struct. Eng.*, **109**(10), 2387-2403.

Kuşyılmaz, A. and Topkaya, C. (2015), "Displacement amplification factors for steel eccentrically braced frames", *Earthq. Eng. Struct. Dyn.*, **44**(2), 167-184.

Li, S., Tian, J.B. and Liu, Y.H. (2017), "Performance-based seismic design of eccentrically braced steel frames using target drift and failure mode", *Earthq. Struct.*, **13**(5), 443-454.

Lian, M. and Su, M.Z. (2017), "Seismic performance of high-strength steel fabricated eccentrically braced frame with vertical shear link", *J. Constr. Steel Res.*, **137**(10), 262-285.

Lian, M. and Su, M.Z. (2017), "Experimental study and simplified analysis of ebf fabricated with high strength steel", *J. Constr. Steel Res.*, **139**(12), 6-17.

Lian, M., Su, M.Z. and Guo, Y. (2015), "Seismic performance of eccentrically braced frames with high strength steel

combination", *Steel Compos. Struct.*, **18**(6), 1517-1539.
Longo, A., Montuori, R., Nastri, E. and Piluso, V. (2014), "On the use of hss in seismic-resistant structures", *J. Constr. Steel Res.*, **103**(12), 1-12.
Richards, P.W. (2004), "Cyclic stability and capacity design of steel eccentrically braced frames", Ph.D. Dissertation, Department of Structural Engineering, University Of California, San Diego.
Shi, G., Hu, F. and Shi, Y.J. (2014), "Recent research advances of high strength steel structures and codification of design specification in china", *Int. J. Steel Struct.*, **14**(4), 873-887.
Tanabashi, R., Naneta, K. and Ishida, T. (1974), "On the rigidity and ductility of steel bracing assemblage", *Proceedings of the 5th World Conference on Earthquake Engineering*, IAEE, Rome.
Tian, X.H., Su, M.Z., Lian, M., Wang, F. and Li, S. (2018), "Seismic behavior of k-shaped eccentrically braced frames with high-strength steel: shaking table testing and FEM analysis", *J. Constr. Steel Res.*, **143**(4), 250-263.
Wang, F., Su, M.Z., Hong, M., Guo, Y. and Li, S.H. (2016), "Cyclic behaviour of y-shaped eccentrically braced frames fabricated with high-strength steel composite", *J. Constr. Steel Res.*, **120**(4), 176-187.

KT

Symbols

θ_y	yield drift
θ_u	ultimate drift
θ_p	plastic drift
μ_s	the structural ductility factor
R_μ	the ductility reduction factor
γ	the energy modification factor
V	the total design base shear
G_j	the seismic weight at level j
H_j	the height of level j from the base
G_n	the weight at the top level
H_n	the height of roof level from base
G	the total weight of the structure
T	the fundamental period
g	the gravitational acceleration
β_i	the shear distribution factor at level i
F_i	the lateral force at level i
F_n	the lateral force at top level
S_a	the spectral acceleration
$\beta_i V_{pr}$	the plastic shear strength of ith story link.
M_{pc}	the plastic moment of column base
L	the span of the EBFs
V_u	the ultimate shear capacity of link
V_p	the plastic shear capacity of link
M_u	the ultimate moment capacity of link
ψ	strength reduction factor
h_1	the bottom story height
ω_i	the vertical force in ith story beams
e	link length
h_i	the ith level story height
V'	one-bay base shear
q_i	the uniformly distributed load in ith level story
$P_{u,i}$	the concentrated force in the top column at the ith level story